A comparison of anisotropic phase-shift-plus-interpolation and reverse-time depth migration methods for tilted TI media

Xiang Du, John C. Bancroft and Larry R. Lines

ABSTRACT

Seismic anisotropy in dipping shale layers causes imaging and positioning problems for underlying structures. Two 2D anisotropic depth migration algorithms, anisotropic phase-shift-plus-interpolation (APSPI) and anisotropic reverse-time (ART), are presented for tilted transversely isotropic media (TTI). These two algorithms inherit the accuracy of wavefield extrapolation migration methods. Based on the analytical solution of the frequency-dispersion equation, APSPI algorithms can handle an arbitrary distribution of velocities and anisotropic parameters. We also derive the P-wave and SV-wave equations for tilted TI media using the frequency-dispersion equation.

APSPI belongs to the downward continuation method that uses one-way wave equation migration methods, while ART is a full wave equation method. We focus our research on the differences between accuracy and efficiency. In addition, we evaluate the difference between isotropic and anisotropic migrations. Examples demonstrate that APSPI and ART have excellent performance for arbitrary velocity and anisotropic parameters media. However ART does not suffer from the dip limitation of one-way downward continuation algorithms.

INTRODUCTION

Velocity measurements in the laboratory (Thomsen, 1986) and field studies (Crampin et. al, 1984) have shown that many sedimentary rocks exhibit anisotropy. Thick anisotropic sequences of dipping sandstones and shales often overlie the reservoir in fold and thrust belts, such as the Canadian Foothills. In these cases, such an assumption, when anisotropy is negligible, may result in imaging problems and mispositioning errors, as studied by Isaac and Lawton (1999). Several authors have recently developed migration methods for anisotropic media. Akhalifah (1995) used a Gaussian beam algorithm for poststack migration in 2D transversely isotropic media with a vertical axis of symmetry (VTI). Le Rousseau (1997) and Ferguson and Margrave (1998) extended the phase-shift-plus-interpolation and non-stationary phase shift method to TTI media. Ristow (1999) presented an implicit 2D depth migration scheme for VTI media based on the coefficients of finite difference (FD) equation. Han (2000) proposed two prestack converted-wave migration algorithms for VTI media, including anisotropic PSPI by analytically solving k_z with the Christoffel equation and anisotropic FD algorithm. Zhang et al. (2001) proposed shot spatial convolution operators to extrapolate the wavefields recursively in the space-frequency domain for qP and qSV-wave in TTI media. Zhang et al. (2002) presented a finite difference (FD) scheme for the computation of first arrival traveltime on regular grids for transversely isotropic (TI) media. Kumar et al. (2004) carried out 2D Kirchhoff migration based on their traveltime algorithms. Du et al. (2005) introduced the anisotropic reverse-time migration for TTI media.

In this paper, we chose two anisotropic migration methods for a comparison, including anisotropic PSPI and anisotropic reverse-time migration. The former is based on one-way downward continue migration methods, while the latter is a full-wave equation migration method. Rather than use an approximated solution of k_z, such as table-driven interpolation (Le Rousseau, 1997) and an interpolation polynomial (Ferguson and Margrave, 1998), we solve k_z analytically from the quartic dispersion equation (see appendix). Starting from a frequency dispersion equation as well, we applied our P-wave equation and SV-wave equation for tilted TI media (Du et al., 2005). A comparison between anisotropic PSPI and ART demonstrates individual performance with respect to accuracy and efficiency. In addition, the extra computer run-time is counted for each migration algorithm when using anisotropic parameters. One numerical and two physical examples demonstrate that the two anisotropic migration methods improve the imaging accuracy and energy focus

THEORY

Anisotropic Phase-shift-plus interpolation migration (APSPI)

Since anisotropic Phase shift plus interpolation migration is derived from PSPI, we first review the basic PSPI approach. Given a homogeneous velocity field in the frequency-wavenumber domain, the 2D acoustic wave equation is given by

$$k_x^2 P - \frac{\partial^2 P}{\partial z^2} = \frac{\omega^2}{v^2} P, \tag{1}$$

where P is the pressure field, z is the depth, ω is the circular frequency, and v is velocity and k_x is the wavenumber in the lateral direction. Taking the Fourier transform in the z direction gives us the frequency dispersion equation

$$k_x^2 + k_z^2 = \frac{\omega^2}{v^2}, \tag{2}$$

and its corresponding one-way wave equation

$$\frac{\partial P}{\partial z} = \pm i k_z P, \tag{3}$$

here the $\pm$ signs correspond to downgoing and upgoing wavefields respectively. Assuming that $v(z)$ is constant over the depth interval dz, we can get the analytic solutions for the one-way wave equation:

$$P(z + \Delta z, k_x, \omega) = e^{\pm i k_z z} P(z, k_x, \omega). \tag{4}$$

Thus the wavefield in depth involves a simple phase shift in the frequency-wavenumber domain. The above theory is actually provided by Gazdag migration (Gazdag, 1978). The advantage of this method is its stability with no special requirement for the grid spacing and its accuracy up to 90^0 degree dips. When the velocity field varies laterally, the phase shift method fails, for it assumes that the velocities vary only with depth z. Thus, Gazdag and Sguazzero (1984) advanced the Phase-shift-plus-interpolation method that used

several reference velocities to account for the lateral velocity variation. At each step, they use several reference velocities to account for the lateral velocity variation. The true wavefield is obtained by linearly interpolating the reference wavefield using the relationship between local velocity and reference velocities.

When the velocity field varies not only with lateral direction but also with the phase angle in anisotropic media, k_z is a function of vertical velocities and anisotropic parameters. Similar to the isotropic case, we have the anisotropic dispersion relationship,

$$k_z = \pm\sqrt{\frac{\omega^2}{v^2(\theta)} - k_x^2}\ , \tag{5}$$

where ω is the frequency, $v(\theta)$ is the angle-dependent velocity, θ is the phase angle with the symmetry axis. For all the phase-shift-based migration algorithms, the key is to relate k_z to k_x with known k_x. In the isotropic case, ω and v are constant, so k_z can be readily computed from k_x, ω and v using the isotropic frequency dispersion equation. In anisotropic media, the angle-dependence of velocity makes the computation more complicated.

According to Tsvankin (1996), the phase velocity $v(\theta)$ can be described in terms of ε, δ, and the vertical P- and SV-wave velocity Vp_0 and Vs_0 as

$$\begin{aligned}\frac{V^2(\theta)}{V_{p0}^2} &= 1+\varepsilon\sin^2\theta - \frac{f}{2} \\ &\pm\frac{f}{2}\sqrt{(1+\frac{2\varepsilon\sin^2\theta}{f})^2 - \frac{2(\varepsilon-\delta)\sin^2 2\theta}{f}}\ .\end{aligned} \tag{6}$$

When we rotate the symmetry axis from vertical to a tilt angle ϕ, the phase velocity in the direction measured from the vertical direction is:

$$\begin{aligned}\frac{V^2(\theta,\phi)}{V_{p0}^2} &= 1+\varepsilon\sin^2(\theta-\phi) - \frac{f}{2} \\ &\pm\frac{f}{2}\sqrt{(1+\frac{2\varepsilon\sin^2(\theta-\phi)}{f})^2 - \frac{2(\varepsilon-\delta)\sin^2 2(\theta-\phi)}{f}}\ ,\end{aligned} \tag{7}$$

where the + and – signs are for P-and SV-waves respectively, and $f = 1-\frac{V_{s0}^2}{V_{p0}^2}$. ε and δ are Thomsen parameters (Thomsen, 1986), which are defined as:

$$\varepsilon = \frac{c_{11} - c_{33}}{2c_{33}};\ \delta = \frac{(c_{13} + c_{44})^2 - (c_{13} - c_{44})^2}{2c_{33}(c_{13} - c_{44})}; \tag{8}$$

where c_{ij} are elastic moduli. With the weak-anisotropic assumption, the expression for the anisotropic phase velocity can be simplified by expanding it to first order in the small parameters ε and δ:

$$\frac{V_p^2(\theta)}{V_{p0}^2} = 1 + 2\delta \sin^2\theta \cos^2\theta + 2\varepsilon \sin^4\theta, \tag{9}$$

$$\frac{V_s^2(\theta)}{V_{s0}^2} = 1 + 2\sigma \sin^2\theta \cos^2\theta, \tag{10}$$

where $\sigma = \frac{V_{p0}^2}{V_{s0}^2}(\varepsilon - \delta)$. Using the Equation (6) as the starting point, Le Rousseau (1997) developed an anisotropic PSPI algorithm for migration wherein he precomputes a table of $k_z(\theta)$ and $k_x(\theta)$ while considering the angle dependence of velocity for anisotropic parameters, locates or interpolates a given input k_x in the table, and finds the corresponding k_z, the accuracy of this table-driven algorithm is directly related to the size of the table; the finer the increment in phase angle θ, the better the result. With the larger table, it is obvious that searching is time-consuming. Ferguson and Margrave (1998) suggested using an interpolating polynomial to get approximated solutions of k_z. They first estimated an empirical polynomial relationship between phase angle θ and horizontal slowness p by a series of numerical experiments, and then used the θ expression to calculation vertical slowness to get k_z. It appears, however, that experiments are cumbersome with difference anisotropic parameters. A difficulty presents itself when the axis of symmetry ϕ of a TI medium is non-zero. The horizontal slowness versus phase angle for dipping TI medium shows that some values of p correspond to two values of θ, so we have to turn to other methods for a remedy.

In fact, we can solve k_z analytically from the quartic dispersion equation (see Appendix) such as

$$k_z^4 + a_3 k_z^3 + a_2 k_z^2 + a_1 k_z^1 + a_0 = 0, \tag{11}$$

where a_i ($i = 0, 1, 2, 3$) is related to k_x, ε, δ, v_{p0} and ϕ. Considering that we are comparing with anisotropic reverse-time migration that uses the weak anisotropy approximation, we get the analytical solution for the P wave. Two roots out of four of the quartic dispersion equation are chosen, corresponding to the down- and upgoing-qP waves, respectively. Figure 1 shows a solution of the quartic dispersion equation for TI medium with a tilted angle of 0, 30, 60, 90 degrees. The analytical solutions are also shown in this figure with cyan color. The numerical solutions exactly match them. The performance of the phase shift operator can best be exemplified through a study of migration impulse responses. Since existing laboratory and field data indicate that the

parameter ε is predominantly positive and most measurements made for transversely isotropic formations at seismic frequencies indicate that $\varepsilon > \delta$ (Thomsen, 1986), we take $\varepsilon = 0.24$ and $\delta = 0.1$. Figure 2 illustrates the impulse response of P wave propagation modes with a tilt angle of 0, 30, 60, 90 degrees. The arrows represent the symmetry axis that has a good correspondence with each tilted angle. Furthermore, the phase shift method exhibits excellent performance in dipping angles up to 90 degrees that is better than the optimum explicit operators by Zhang et al. (2001).

As in the isotropic PSPI algorithm, several sets of reference parameters must be used for the migration. Ideally, reference wavefields would be generated for each set of reference parameters. Considering that we used four Thomsen parameters v_{p0}, ε, δ and ϕ, we would require 625 different sets of reference parameters. To make computation affordable, it is assumed that parameters v_{p0}, ε and δ have correlated lateral variation. Since tilt angle ϕ has a big effect on the wavefront dip direction, we take full account of the tilt angle. For anisotropic PSPI, balancing the computation cost and the number of reference parameters remains an unresolved issue. The same issue of treating independent lateral variations in all four Thomsen parameters exists for a lot of anisotropic algorithms such as a phase-shift operator, and for explicit downward-continuation methods (Uzcategui, 1994).

Anisotropic reverse-time migration (ART)

Since Du et al., (2005) presented anisotropic reverse-time migration, we do not present much detailed analysis here and just review it quickly. In the same way, we start from VTI phase-velocity equation (Tsvankin, 1996) written as

$$\frac{V^2(\theta)}{V_{p0}^2} = 1 + \varepsilon \sin^2\theta - \frac{f}{2} \pm \frac{f}{2}\sqrt{\left(1 + \frac{2\varepsilon \sin^2\theta}{f}\right)^2 - \frac{2(\varepsilon - \delta)\sin^2 2\theta}{f}} \tag{12}$$

Under the assumption of weak anisotropy, we transform the phase-velocity equation (12). Expanding the radical in Taylor Series and dropping terms quadratic in the anisotropies ε and δ, we can obtain the P-wave and SV-wave phase velocity formula as:

$$\frac{V_p^2(\theta)}{V_{p0}^2} = 1 + 2\delta \sin^2\theta \cos^2\theta + 2\varepsilon \sin^4\theta \tag{13}$$

$$\frac{V_s^2(\theta)}{V_{p0}^2} = 1 - f + 2(\varepsilon - \delta)\sin^2\theta \cos^2\theta \tag{14}$$

By rotating the symmetry axis from vertical to a tilt angle ϕ, we can get the phase velocity for P and SV waves in the direction measured from the vertical direction. The P and SV phase velocity measured from a horizontal plane are shown as follows:

$$\frac{V_p^2(\theta,\phi)}{V_{p0}^2} = 1 + 2\delta \sin^2(\theta-\phi)\cos^2(\theta-\phi) + 2\varepsilon \sin^4(\theta-\phi) \tag{15}$$

$$\frac{V_s^2(\theta)}{V_{p0}^2} = 1 - f + 2(\varepsilon-\delta)\sin^2(\theta-\phi)\cos^2(\theta-\phi) \tag{16}$$

For plane waves traveling in the vertical (x, z)-plane, the phase angle is given by

$$\sin\theta = \frac{v(\theta,\phi)k_x}{\omega}, \quad \cos\theta = \frac{v(\theta,\phi)k_z}{\omega} \tag{17}$$

When we multiply Equation (15) and (16) with the wavefields in the Fourier domain, and apply an inverse Fourier transform with ($k_x \to -i\frac{\partial}{\partial x}$, $k_z \to -i\frac{\partial}{\partial z}$, $\omega \to i\frac{\partial}{\partial t}$), we can obtain the P-wave equation and SV-wave equation in tilted transversely isotropic media. The P wave equation for tilted transverse isotropic media is

$$\begin{aligned}\frac{\partial^2 U_p(k_x,k_z,t)}{\partial t^2} = -V_{p0}^2[&k_x^2 + k_z^2 + (2\delta\sin^2\phi\cos^2\phi + 2\varepsilon\cos^4\phi)\frac{k_x^4}{k_x^2+k_z^2} \\ &+ (2\delta\sin^2\phi\cos^2\phi + 2\varepsilon\sin^4\phi)\frac{k_z^4}{k_x^2+k_z^2} \\ &+ (-\delta\sin^2 2\phi + 3\varepsilon\sin^2 2\phi + 2\delta\cos^2\phi)\frac{k_x^2k_z^2}{k_x^2+k_z^2} \\ &+ (\delta\sin 4\phi - 4\varepsilon\sin 2\phi\cos^2\phi)\frac{k_x^3k_z}{k_x^2+k_z^2} \\ &+ (-\delta\sin 4\phi - 4\varepsilon\sin 2\phi\sin^2\phi)\frac{k_z^3k_x}{k_x^2+k_z^2})]U_p(k_x,k_z,t)\end{aligned} . \tag{18}$$

The SV wave equation for tilted transverse isotropic media is

$$\begin{aligned}\frac{\partial^2 U_s(k_x,k_z,t)}{\partial t^2} = -V_{s0}^2[&k_x^2 + k_z^2 + \frac{\sigma}{2}(2\sin^2 2\phi\frac{k_x^4+k_z^4-2k_x^2k_z^2}{k_x^2+k_z^2} + 4\cos^2\phi)\frac{k_x^2k_z^2}{k_x^2+k_z^2} \\ &+ 4\varepsilon\sin 2\phi\cos^2\phi)\frac{k_xk_z(k_x^2-k_z^2)}{k_x^2+k_z^2}]U_s(k_x,k_z,t) \\ \sigma = (\frac{V_{p0}}{V_{s0}})^2(\varepsilon-\delta)\end{aligned} .(19)$$

The P- and SV-wave equations (Equation 18 and 19) can also be written in the time-space domain. However, space and time are coupled in the terms $\partial^4 u/\partial x^2\partial t^2$ and $\partial^4 u/\partial z^2\partial t^2$, and these cause computational difficulty in finite difference schemes, whereas the equations are easily solved in the time-wavenumber domain. Therefore the pseudospectral method is selected for reverse-time migration (RTM). The pseudospectral method (Fornberg, 1987) is a higher accuracy method that needs fewer grid points per wavelength to obtain any desired accuracy. It successfully solves the frequency dispersion problem which results from a limited difference operator in reverse-time migration. In the numerical computation, we apply the phase shift in the

wavenumber domain, change the velocity and anisotropic parameters (ε, δ and ϕ) in the spatial domain, and transform to the wavenumber domain again in time steps. The algorithm is capable of being adapted to arbitrary heterogeneous velocities and parameters. The algorithm procedure is shown in Figure 3.

Relationship between the APSPI and ART

As stated in the introduction about anisotropic phase-shift-plus-interpolation and anisotropic reverse-time theory, we can find two isotropic methods which can be successfully extended to be used in tilted transversely isotropic media. Anisotropic PSPI performs computations in the wavenumber and frequency domain that result in interpolating the wavefield in the spatial domain to accommodate the velocity variation along the lateral direction. In contrast to algorithms using approximation of the one-way wave equation, such as explicit operators and implicit operators in x-ω domain, APSPI maintains high accuracy for dip angle up to and beyond 90 degrees and has less numerical noise caused by approximation as well. Furthermore, it is straightforward to extend from 2D to 3D, involving only an additional Fourier transform in the y-direction. Anisotropic reverse-time migration preserves the full dip angle and overturned reflection imaging ability in that it is two-way wave equation solution. In addition, it automatically adapts to variation of velocities and anisotropic parameters in the spatial domain. In fact, the step-by-step reverse calculation also makes the algorithm expensive. From the comparison, APSPI makes a good balance between accuracy and efficiency while ART justifies its accuracy especially in complex media.

EXAMPLES

To show the difference between the two migration methods, we chose three examples for analysis, including one numerical model and two physical models. The numerical variable velocity model is designed to exhibit the accurate dip angle imaging ability difference between APSPI and ART migration in TTI media. Two scaled physical models, an isotropic reef with a TTI overburden and a TTI thrust sheet in an isotropic background, were constructed by the University of Calgary Foothills Research Project (FRP). These models were used to investigate the magnitude of the imaging error incurred by the use of isotropic processing code when there is seismic velocity anisotropy presented in the dipping overburden. The transducer dimensions of the modeling equipment prevented the acquisition of data of true zero offset. However, we can assume that if the near-offset is close enough to zero, it will be consider zero-offset. Migrations of the collected seismic data exhibit the accurate image positioning of two anisotropic migrations while isotropic migration gives considerable errors in physical position and energy focus. Our migration analysis is done in a PC machine with 2.4GHz CPU and 512MB of RAM

Anisotropic imaging reflectors with different angles for variable velocity model

A variable velocity model that consists of six dipping reflectors (0, 15, 30, 45, 60, 75, 90 degrees) is shown in Figure 4. The medium has anisotropic parameters $\varepsilon = 0.2$, $\delta = 0.1$ and the tilt angle is 0. The vertical velocity of the model is $v(x, z) = 1500 + 0.3z + 0.1x$ (m/s). Figure 5 shows a synthetic zero offset section for this model. It was generated by a SU (Seismic Unix software available from Center for Wave Phenomena,

Colorado School of Mines) anisotropic modeling code that treats transversely isotropic media. Figure 6 is the isotropic migration result obtained from isotropic reverse-time migration method of 8^{th} order accuracy. Figure 7 corresponds to isotropic PSPI. There is hardly any difference between the two isotropic migration algorithms and the results are undermigrated without considering anisotropic situation. Correct imaging results are shown in Figure 8 and 9 by anisotropic PSPI and anisotropic RT migration algorithms with exact anisotropic parameters, respectively. In addition, the energy for the reflector with 90^0 dipping angle is weak for APSPI migration result while the one for ART is obvious. The energy for reflectors with 75^0 and 60^0 by ART are stronger than that by APSPI. So ART shows excellent ability in dipping angle imaging. It should be mentioned that APSPI cost 5 minutes to finish the computation while ART used 8 minutes. It seems that APSPI makes a balance between the accuracy and efficiency. The overall comparison of computational cost is shown in Figure 10. It costs 4 minutes and 5 minutes for isotropic PSPI and RT. When we compare the computer run-time between isotropic and anisotropic cases for each of the two algorithms, since homogenous anisotropic parameters case is designed, the computation increment doesn't change more.

Depth migration for isotropic reef with a TTI overburden

Seismic data from an anisotropic physical model described by Isaac and Lawton (1999) were used to test the migration algorithm. The cross-section of this model is shown in Figure 11; it includes a TTI overburden layer, 1500m thick, with the axis of symmetry dipping at 45^0. The layer has parameters Vp_0 = 2950m/s, $\varepsilon = 0.241$, and $\delta = 0.100$. An isotropic layer that contains a simulated reef edge with Vp_0 = 2740m/s underlies this anisotropic overburden. Figure 12 shows a zero-offset seismic section with the surface wave muted. To make the first interface of the model migrate to the correct position in the isotropic migration, we consider that the dipping angle is 45^0 and adopt V_{45} for the upper layer. Migration results of the zero-offset section by isotropic PSPI and RT migration yield an image of the reef edge which is displaced by about 350m to the left of its true position (Figure 13 and Figure 15). Migration by anisotropic RT and anisotropic PSPI algorithms correctly positions the edge of reef, as shown in Figure 14 and 16. In addition, we can find that there is some reflection alias for RT migration from Figure 14 and Figure 16 because of velocity interfaces, which can be removed by smoothing the velocity model. From the two anisotropic migration results, there is very little difference in the migration quality. As for the efficiency, isotropic PSPI, isotropic reverse-time migration, isotropic PSPI and anisotropic PSPI cost 3 minutes, 5 minutes, 7 minutes, and 20 minutes. Since the tilt angle is 45^0, it appears that it increases the required computation more for anisotropic PSPI than for isotropic PSPI. As for ART migration, the computer run-time is more expensive than APSPI, which can be found from Figure 17.

Migration for TTI thrust sheet in an isotropic background

The second physical model is that of a flat reflector overlain by a TI thrust sheet embedded in an isotropic background. The model is shown in Figure 18. The thrust sheet is composed of four blocks in the model; each with a unique axis of symmetry. They have parameters of Vp_0 = 2925m/s, $\varepsilon = 0.224$ and $\delta = 0.100$. The isotropic background

has a flat basement with Vp_0 = 2740m/s. The zero-offset seismic section is given in Figure 19. Figures 20 and 22 are isotropic and anisotropic PSPI migration results. Figures 21 and 23 correspond to isotropic and anisotropic reverse-time migration results. The blue lines in the four figures denote the true location of the thrust sheet interfaces. With the velocity Vp_0 = 2925m/s for the thrust sheet, the isotropic PSPI and RT migration results (Figure 19 and Figure 21) produce a partially flat basement, whereas the basement beneath thrust sheets exhibits substantial pull up and the energy cannot be focused. The interface between the block with 60 degrees tilted angle and the block with 51 degrees tilted angle is incorrectly positioned since the black solid line does not match with the migration event. Migration results by anisotropic PSPI and RT migration (Figure 20 and Figure 22) show more accurate positioning of the reflectors and have nearly flattened the basement reflection, although the reflection event is not continuous. The interface reflection interference of the base reflector between 2000m and 3300m is believed to indicate a shadow zone caused by the high-velocity thrust sheet overlying slower material. The shadow zone is a result of the zero-offset geometry of the recording. In fact, migration of the prestack data by source-gather migration will fill in the shadow zone due to the multiplicity of ray paths afforded by the prestack geometry, which can be seen from Figure 24, created by anisotropic prestack PSPI migration. Due to a more complex physical model, the anisotropic algorithms greatly increase the computation consumption. Isotropic PSPI uses 4 minutes whereas anisotropic PSPI almost takes 15 minutes. Similar to PSPI methods, isotropic reverse-time migration employs 6 minutes, but anisotropic reverse-time migration uses almost 30 minutes. The efficiency comparisons are shown in Figure 25. However, when we compared the anisotropic PSPI and RT results, there is no obvious difference between them due to the fact that we only deal with the poststack seismic data. Some noise exists in the APSPI migration result. With the anisotropic prestack reverse-time migration, the dipping reflector should be clearly imaged, which will be confirmed in the future.

CONCLUSIONS

From the above analysis, it is obvious that anisotropy has a large influence on the accuracy of migrated images. Use of a migration algorithm that takes anisotropy into account, with correct velocity information, can substantially improve images when anisotropy is present. In this paper, the anisotropic PSPI algorithm theory for TTI media is introduced and a new way to get an analytical solution for vertical wavenumber is presented. Anisotropic reverse-time migration theory is also reviewed here, and at the same time we present an appropriate P- and S-wave equation to use in place of the isotropic acoustic wave equation employed in isotropic reverse-time migration. The pseudo-spectral method is easily used to solve these equations implementing reverse-time migration. With numerical and physical examples, we give an overall analysis for two algorithms not only between anisotropic algorithms, but also between individual isotropic migration and anisotropic migration with the aspect to both accuracy and efficiency. From the result comparison, we find anisotropic PSPI and anisotropic RT are both encouraging and promising. The anisotropic RT migration algorithm shows excellent capability in dip angle imaging, whereas anisotropic PSPI keeps a good balance between accuracy and efficiency. Anisotropic PSPI uses almost twice as much computation as isotropic PSPI, while the computational cost of anisotropic RT is nearly five times as large as that of isotropic RT. However, with the rapid development of computer

hardware, all kinds of anisotropic depth migration algorithms will be widely used in seismic imaging.

ACKNOWLEDGEMENTS

We express our thanks to Dr Don Lawton who gave us many suggestions and Dr. Helen Isaac who prepared the model data; and thanks to CREWES for financial support and the SEG for scholarships. We appreciate Center for Wave Phenomena (CWP), Colorado School of Mines for use of free Seismic Unix software.

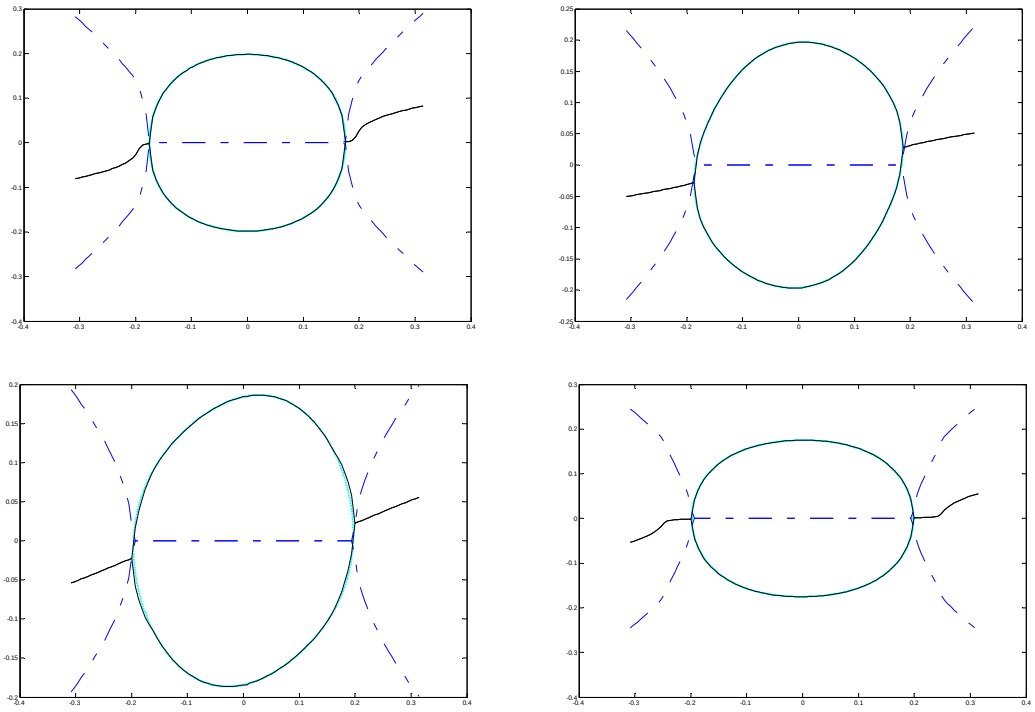

FIG. 1. Dispersion relationship of P-wave for a TI medium. (a), (b), (c) and (d) correspond to the result of a tilt angle of 0, 30, 60, and 90 degrees. The black solid lines denote the real part of k_z, the blue dashed lines are imaginary part of k_z and the cyan solid lines represent the analytical solutions for real part of k_z.

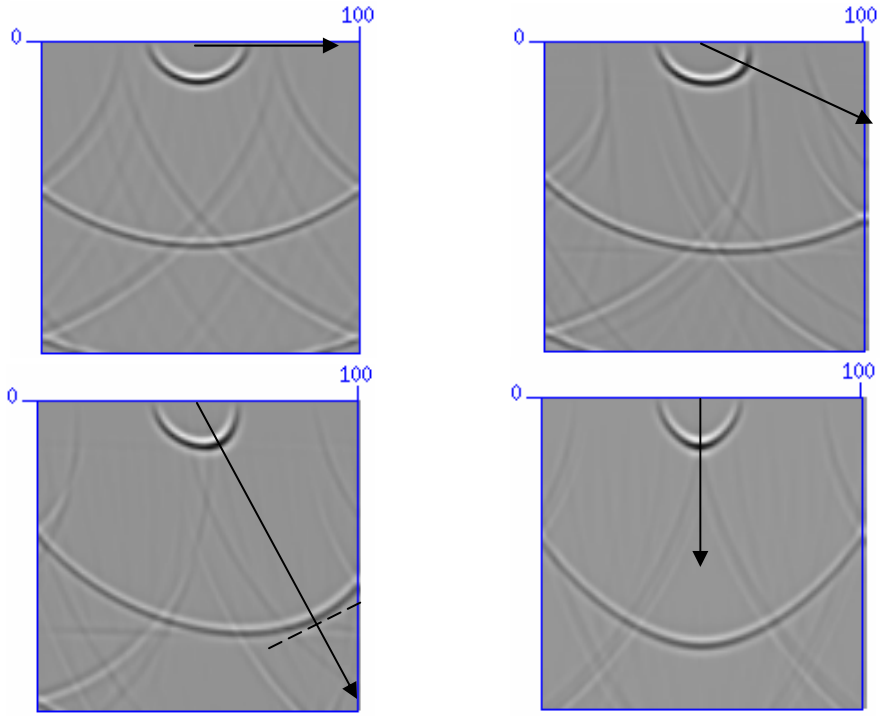

FIG. 2. P- wave impulse response. (a), (b),(c) and (d) correspond to the result of a tilt angle of 0, 30, 60, and 90 degrees as indicated by the arrows.

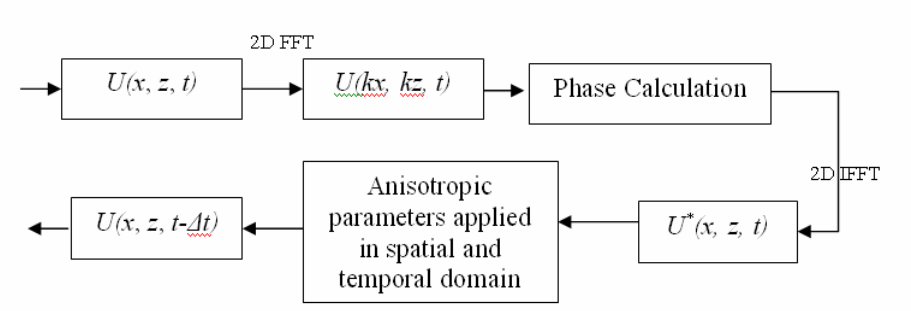

FIG. 3. Computation diagram of anisotropic reverse-time scheme corresponding to equation (18) and (19).

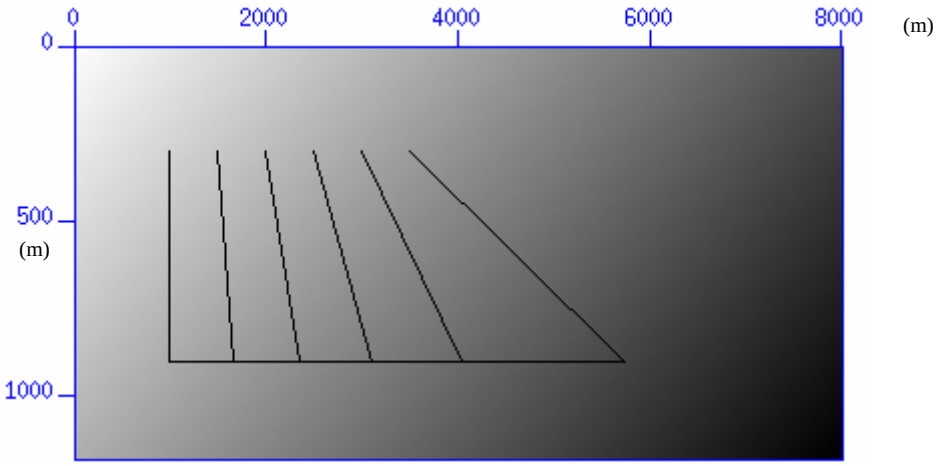

FIG. 4. Variable velocity model with different dipping reflectors.

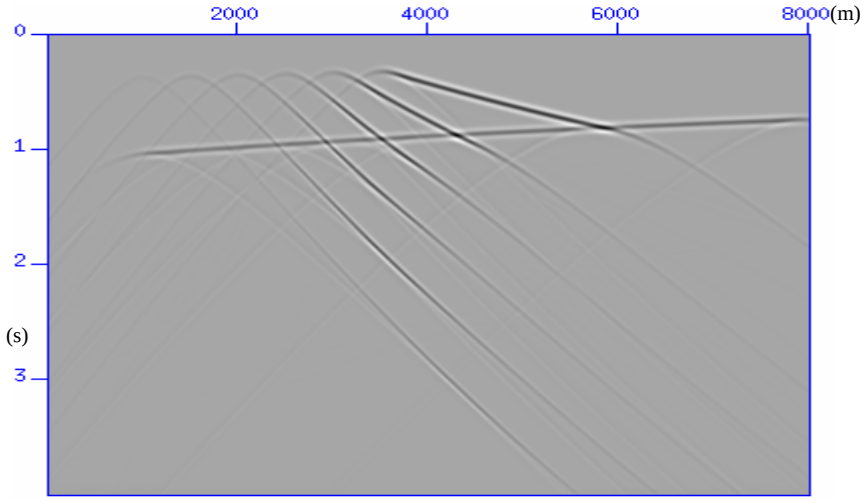

FIG. 5. Synthetic zero-offset seismogram obtained using an SU code from Center for Wave Phenomena (CWP) for the structural model of Figure 4 for TI media.

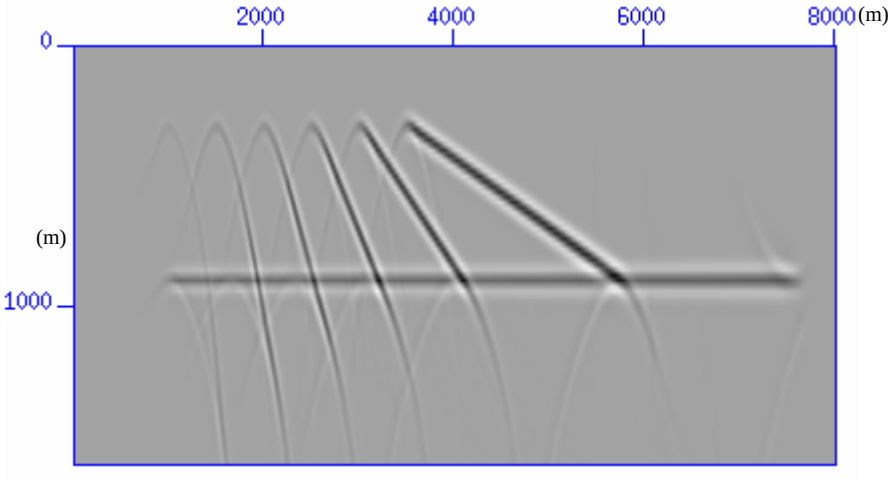

FIG. 6. Isotropic PSPI migration result.

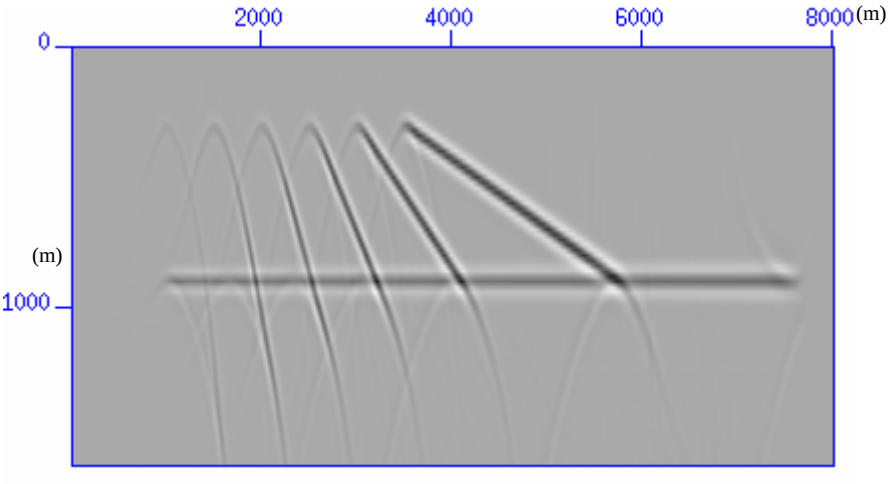

FIG. 7. Isotropic RT migration result.

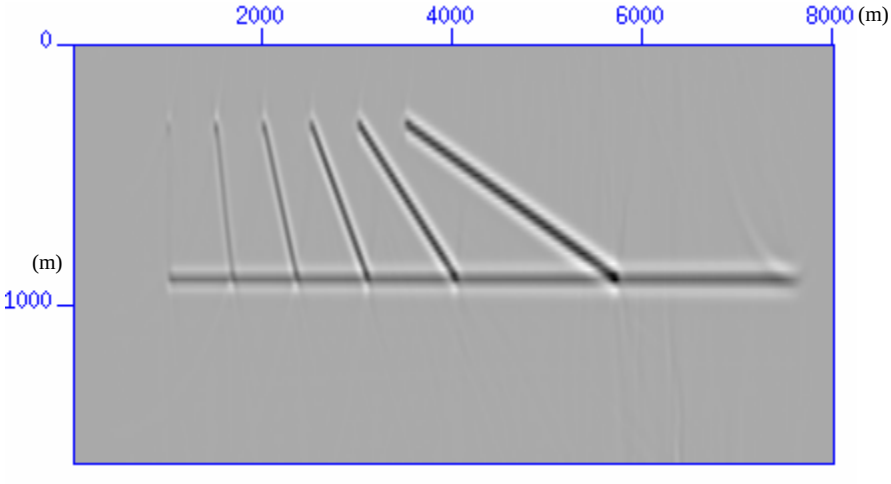

FIG. 8. Anisotropic PSPI migration result.

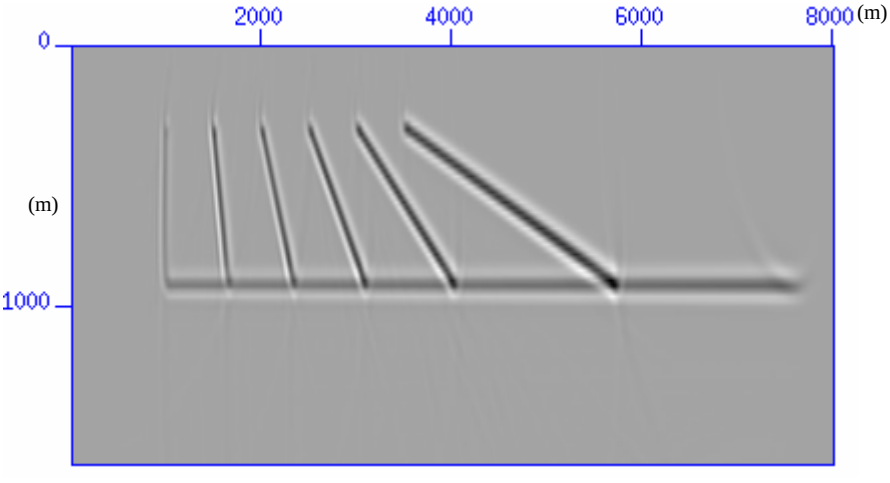

FIG. 9. Anisotropic RT migration result.

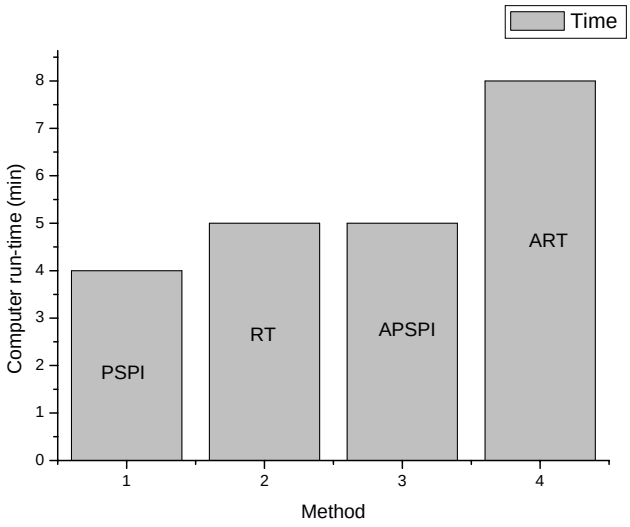

FIG. 10. The efficiency comparison among PSPI, RT, APSPI, ART.

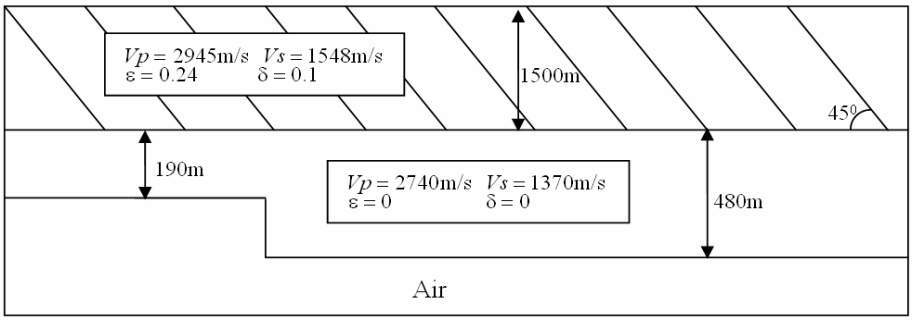

FIG. 11. Isotropic reef with a TTI overburden.

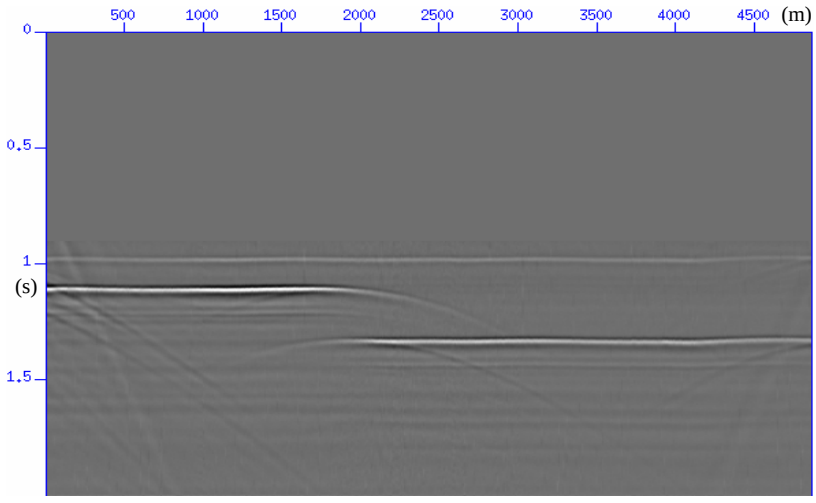

FIG. 12. Zero-offset seismic section of reef model.

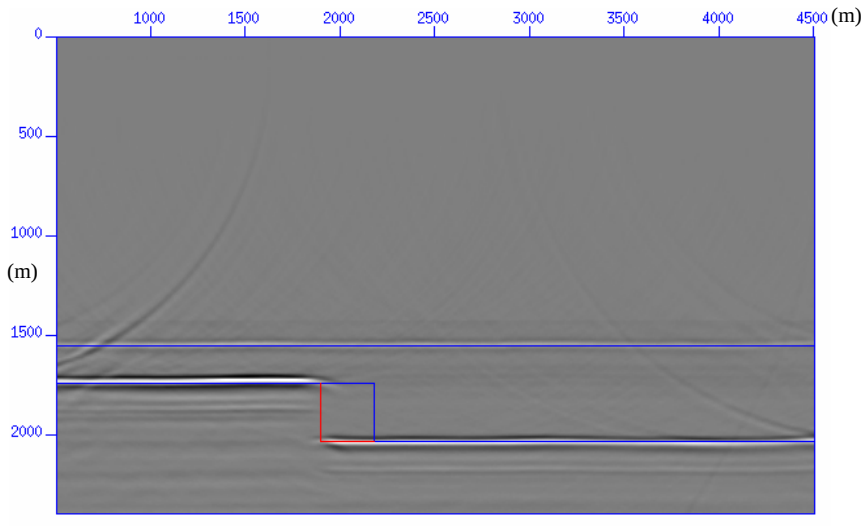

FIG. 13. Isotropic PSPI migration result for reef model.

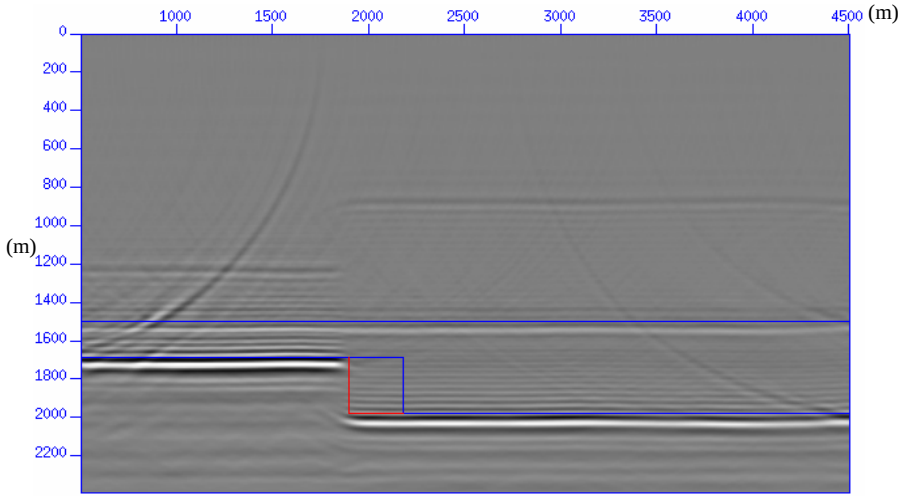

FIG. 14. Isotropic RT migration result of the 6th order accuracy for reef model.

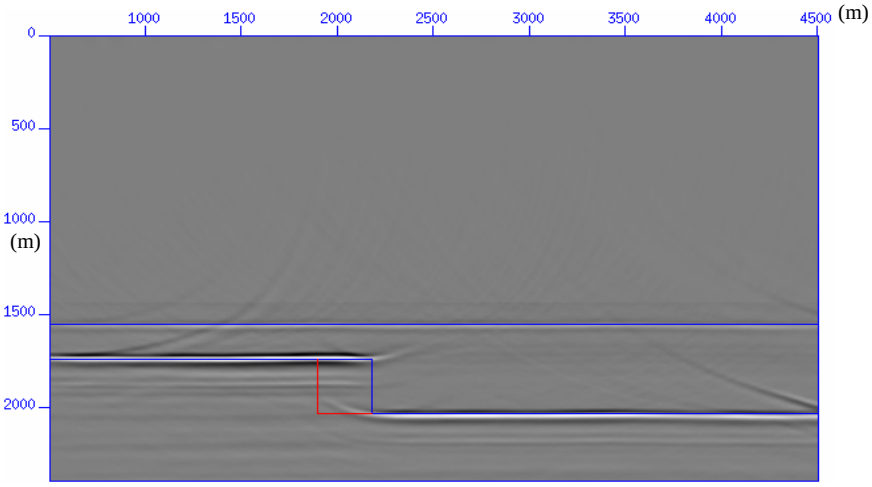

FIG. 15. Anisotropic PSPI migration result for reef model.

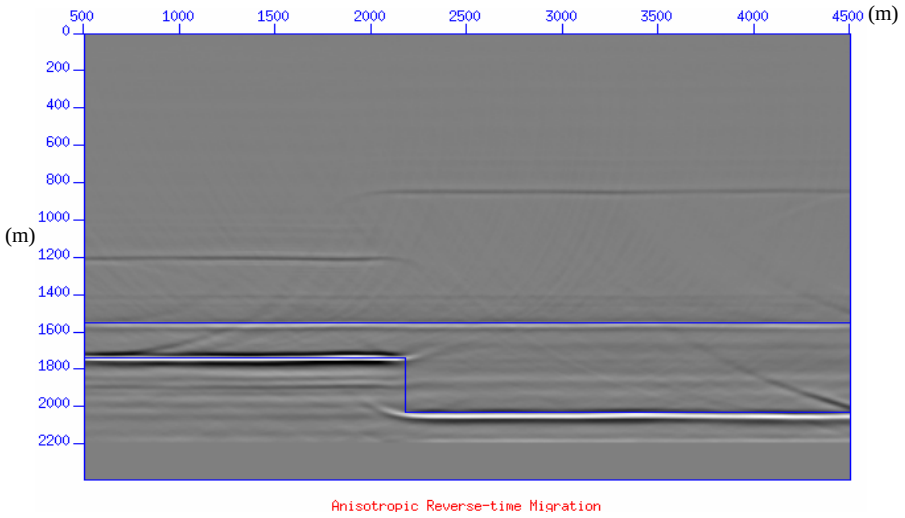

FIG. 16. Anisotropic RT migration result for reef model.

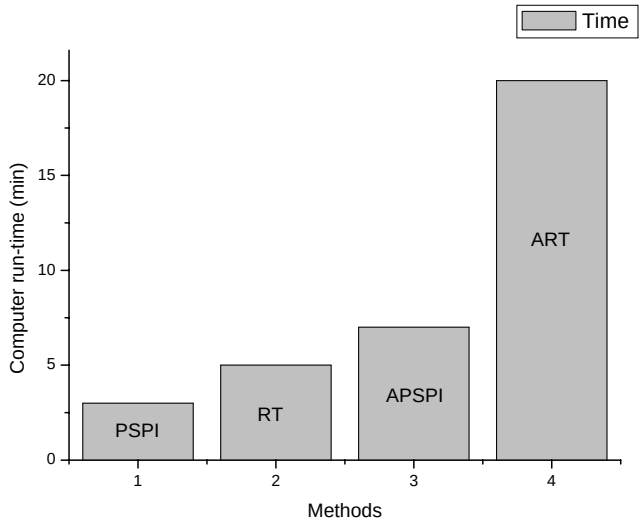

FIG. 10. The efficiency comparison among PSPI, RT, APSPI, ART for reef model.

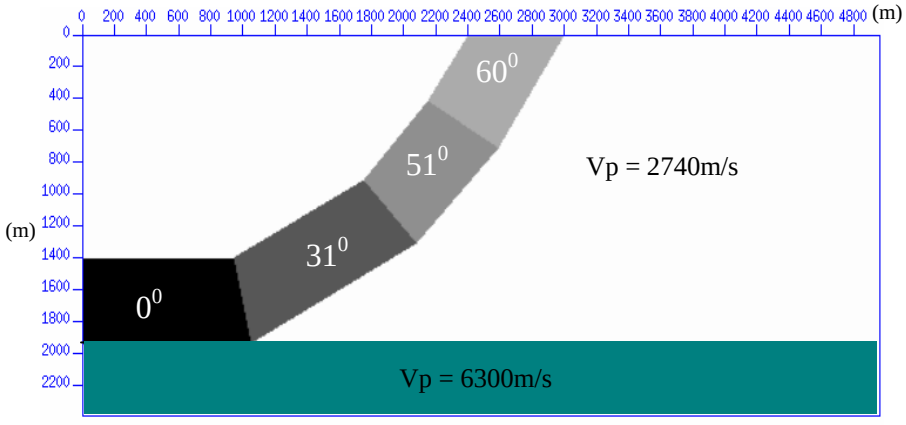

FIG. 18. TTI thrust model.

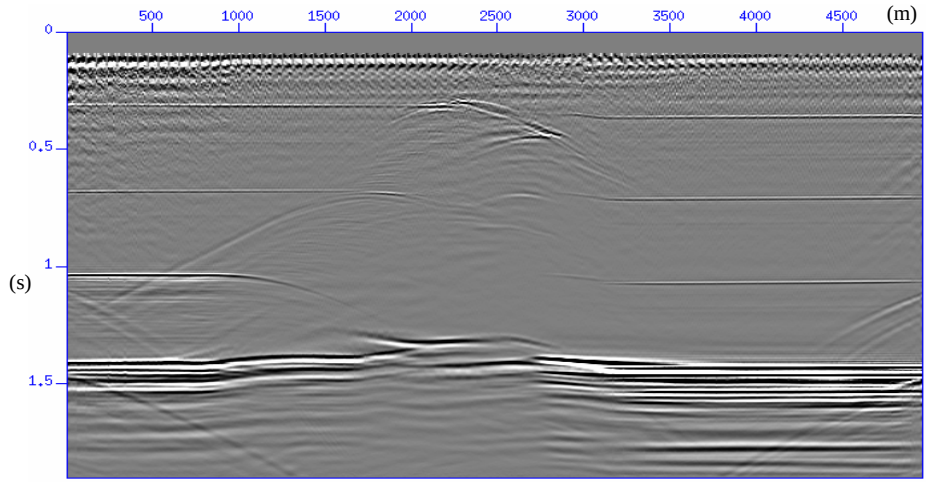

FIG. 19. Zero-offset seismic section of TTI thrust model.

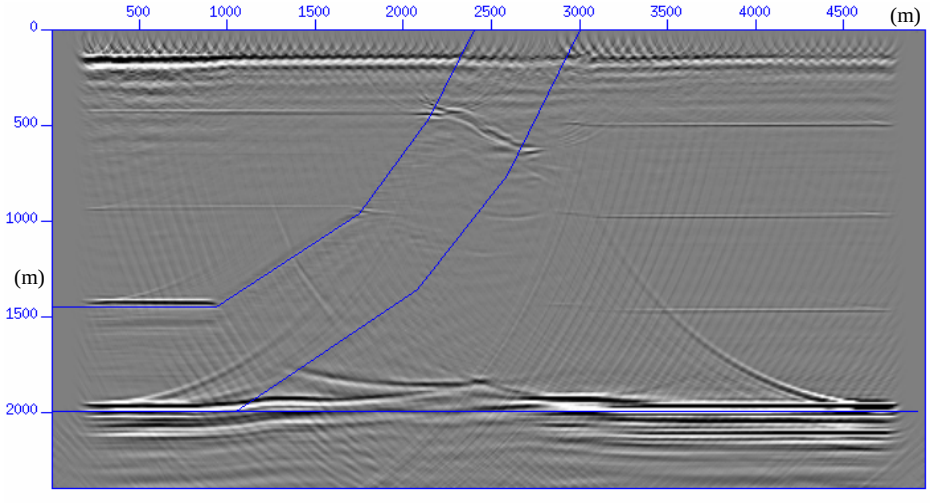

FIG. 20. Isotropic PSPI migration result of TTI thrust model.

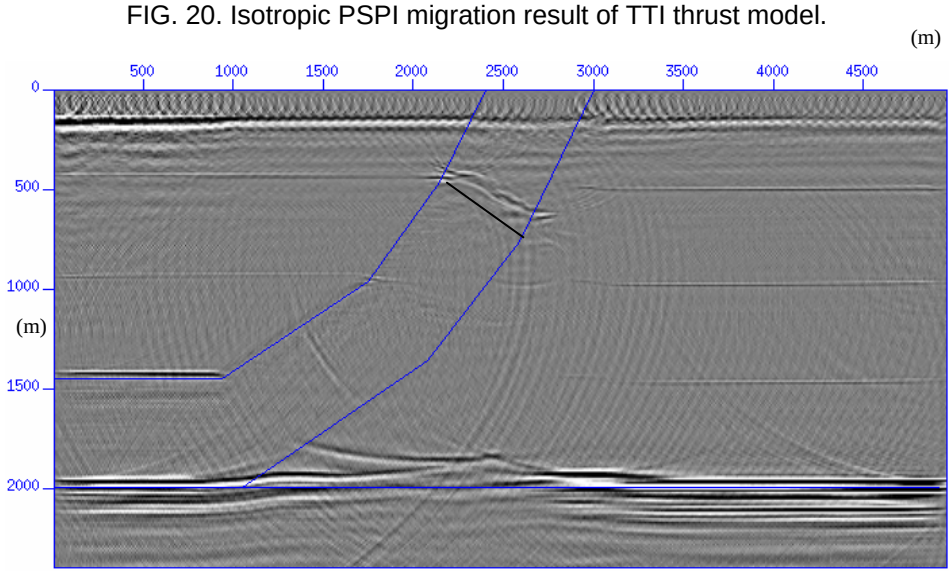

FIG. 21. Isotropic reverse-time migration result of TTI thrust model.

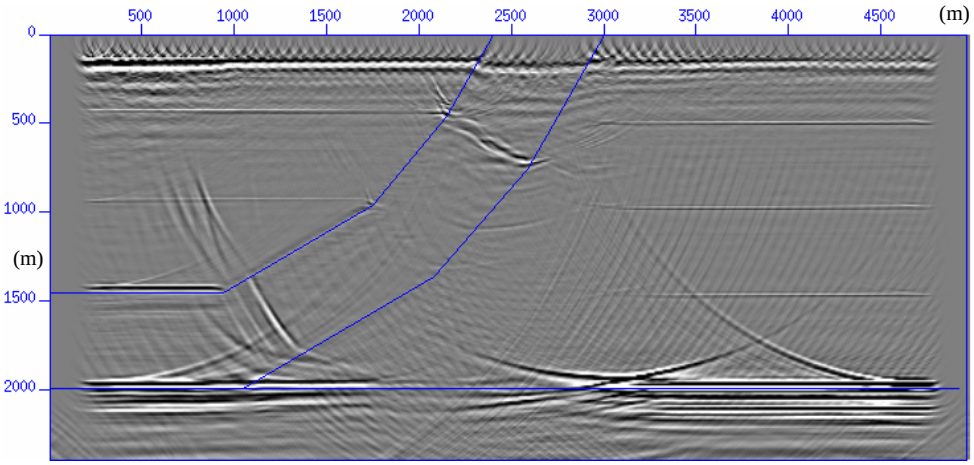

FIG. 22. Anisotropic PSPI migration result of TTI thrust model.

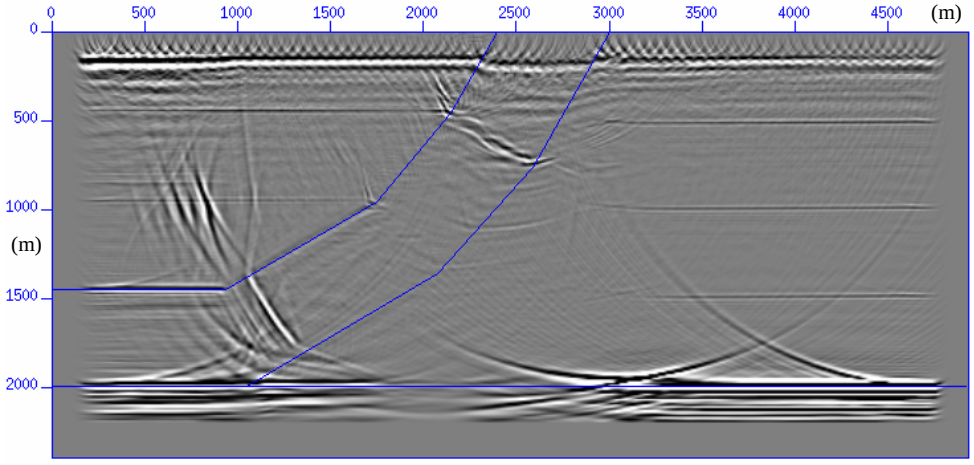

FIG. 23. Anisotropic reverse-time migration result of TTI thrust model.

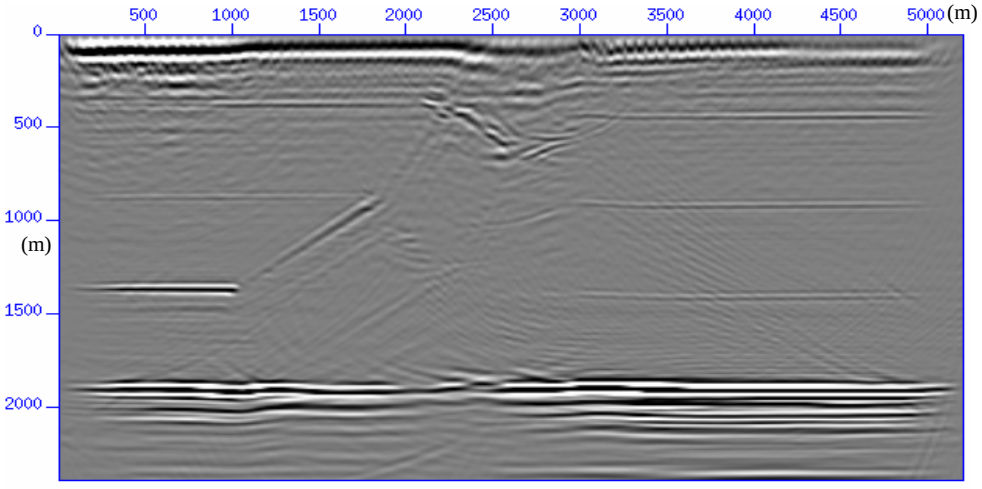

FIG. 24. Anisotropic prestack PSPI migration result of TTI thrust model.

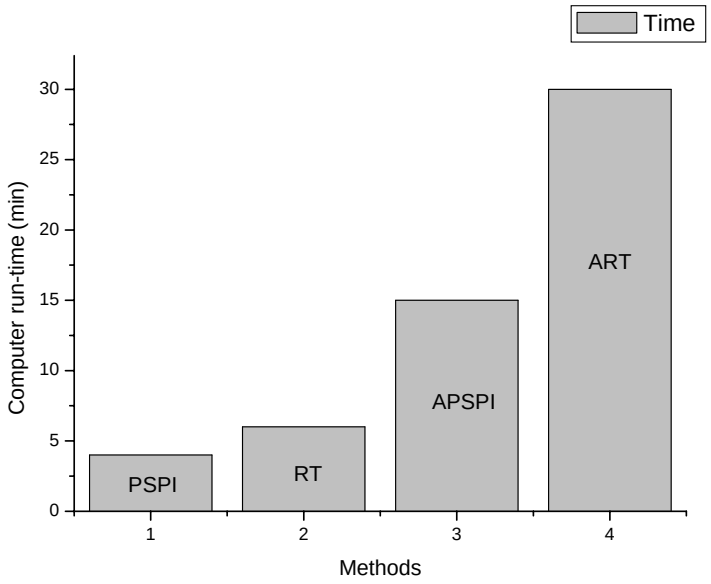

FIG. 25. The efficiency comparison among PSPI, RT, APSPI, ART for thrust model.

REFERENCES

Abramowitz M. and Stegun I. A., 1970, Handbook of mathematical functions. Dover Publications, Inc.

Alkhalifah, T., 1995, Gaussian beam depth migration for anisotropic media: Geophysics, **60**, 1474-1484.

Alkhalifah, T., 2000, An acoustic wave equation for anisotropic media: Geophysics, **65**, 1239-1250.

Crampin, S., Chesnokov, E. M., and Hipkin, R. A., 1984, Seismic anisotropy—The state of the art: First Break, **20**, 9–18.

Daley, P. F, and Lines, L. R., 2004, Linearized quantities in transversely isotropic media, Canadian Journal of Earth Sciences, V.41, 349-354.

Du X., Bancroft J. C. and Lines L. R., 2005, Reverse-time migration for tilted TI media: 75th Mtg. Soc. Expl. Geophys., Expanded Abstracts.

Ferguson, R. and Margrave G. F., 1999, Depth migration in TI media by non-stationary phase shift. 68th SEG meeting, New Orleans, U.S.A., Expanded Abstracts, 1831-1834.

Fornberg, B. 1987, The pseudospectral method - Comparisons with finite differences for the elastic wave equation: Geophysics, **52**, 483-501.

Gazdag, J. 1978, Wave equation migration with the phase shift method. Geophysics, **43**, 1342-1351.

Gazdag, J., and Sguazzero, P. 1984, Migartion of seismic data by phase shift plus interpolation. Geophysics, **49**, 124-131.

Han, B. L., Two prestack converted-wave migration algorithms for vertical transverse isotropy: 70th Mtg. Soc. Expl. Geophys., Expanded Abstracts, 461-464.

Isaac, J. H., and Lawton, D. C., 1999, Image mispositioning due to dipping TI media: A physical seismic study: Geophysics, **64**, 1230-1238.

Kumar D. Sen M. K. and Ferguson R. J., 2004, Traveltime calculation and prestack depth migration in tilted transversely isotropic media. Geophysics, **69**, 37-44.

Le Rousseau, J. H., 1991, Phase shift –based migration for transverse isotropy: 61st Mtg. Soc. Expl. Geophys., Expanded Abstracts, 993-996.

Ristow D. and Rühl T., 1997, Migration in transversely isotopic media using implicit operators: 67th Mtg. Soc. Expl. Geophys., Expanded Abstracts, 1699-1702.

Thomsen, L., 1986, Weak elastic anisotropy: Geophysics, **51**, 1954–1966.

Tsvankin, I., 1996, P-wave signatures and notation for transversely isotropic media: An overview: Geophysics, **61**, 467-483.

Uzcategui, O., 1995, Depth migration in transversely isotropic media with explicit operators.: Geophysics, **60**, 1819-1829.

Zhang, J., Verschuur, D. J. and Wapenaar, C. P. A., 2001, Depth migration of shot records in heterogeneous, tranversely isotropic media using optimum explicit operators: Geophys. Prosp., **49**, 287-299.

Zhang, L., Rector, J. W., and Hoversten, G. M., 2002, An eikonal solver in tilted TI media: 72nd Annual International Meeting, SEG, Expanded Abstracts, 1955–1958.

APPENDIX A

Quartic dispersion equation for P wave in weak anisotropy media and its analytical solution

The frequency dispersion relationship can be described as the following equation

$$\begin{aligned}(k_x^2+k_z^2)\frac{\omega^2}{v_{p0}^2} = (k_x^2+k_z^2)^2 &+(2\delta\sin^2\phi\cos^2\phi+2\varepsilon\cos^4\phi)k_x^4\\ &+(2\delta\sin^2\phi\cos^2\phi+2\varepsilon\sin^4\phi)k_z^4\\ &+(-\delta\sin^2 2\phi+3\varepsilon\sin^2 2\phi+2\delta\cos^2 2\phi)k_x^2k_z^2\\ &+(\delta\sin 4\phi-4\varepsilon\sin 2\phi\cos^2\phi)k_x^3k_z\\ &+(-\delta\sin 4\phi-4\varepsilon\sin 2\phi\sin^2\phi)k_xk_z^3\end{aligned}.$$

To simplify the expression, it can be written as the following quartic equation

$$k_z^4+a_3k_z^3+a_2k_z^2+a_1k_z+a_0=0, \qquad \text{(A1)}$$

where

$$a_4=2\delta\sin^2\phi\cos^2\phi+2\varepsilon\sin^4\phi+1,$$

$$a_3=(-\delta\sin 4\phi-4\varepsilon\sin 2\phi\sin^2\phi)k_x/a_4,$$

$$a_2=[(-\delta\sin^2 2\phi+3\varepsilon\sin^2 2\phi+2\delta\cos^2\phi+2)k_x^2-\frac{\omega^2}{v_{p0}^2}]/a_4,$$

$$a_1=(\delta\sin 4\phi-4\varepsilon\sin 2\phi\cos^2\phi)k_x^3/a_4,$$

and

$$a_0=[(2\delta\sin^2\phi\cos^2\phi+2\varepsilon\cos^4\phi+1)k_x^4-\frac{\omega^2}{v_{p0}^2}k_x^2]/a_4.$$

To get the analytical solution, we try to find the real root of the cubic equation,

$$u^3-a_2u^2+(a_1a_3-4a_0)u-(a_1^2+a_0a_3^2-4a_0a_2)=0, \qquad \text{(A2)}$$

and determine the four roots of the quartic as solutions of the two quadratic equations (Abarmowitz and Stegun, 1970),

$$v^2+[\frac{a_3}{2}\mp(\frac{a_3^2}{4}+u_1-a_2)^{\frac{1}{2}}]+\frac{u_1}{2}\mp[(\frac{u_1}{2})^2-a_0]^{\frac{1}{2}}=0. \qquad \text{(A3)}$$

Considering the cubic equation $z^3+a_2z^2+a_1z+a_0=0$, let

$$m = \frac{1}{3}a_1 - \frac{1}{9}a_2^2, \quad n = \frac{1}{6}(a_1 a_2 - 3a_0) - \frac{1}{27}a_2^3.$$

If $m^3 + n^2 > 0$, one real root and a pair of complex conjugate roots.

If $m^3 + n^2 = 0$, all roots real and at least two are equal.

If $m^3 + n^2 < 0$, all roots real.

As for cubic equation (A2), the three roots are given as follows (Abramowitz and Stegun, 1970): Let

$$s_1 = [r + (q^3 + r^2)^{\frac{1}{2}}]^{\frac{1}{3}}, \; s_2 = [r - (q^3 + r^2)^{\frac{1}{2}}]^{\frac{1}{3}}$$

where

$$q = \frac{1}{3}a_1 a_3 - \frac{1}{9}a_2^2 - \frac{4}{3}a_0, \quad r = \frac{1}{27}a_2^3 + \frac{1}{2}a_1^2 + \frac{1}{2}a_0 a_3^2 - \frac{4}{3}a_0 a_2 - \frac{1}{6}a_1 a_2 a_3.$$

Then

$$R_1 = (s_1 + s_2) + \frac{a_2}{3},$$

$$R_2 = \frac{1}{2}(s_1 + s_2) + \frac{a_2}{3} + \frac{i\sqrt{3}}{2}(s_1 - s_2),$$

and

$$R_3 = \frac{1}{2}(s_1 + s_2) + \frac{a_2}{3} - \frac{i\sqrt{3}}{2}(s_1 - s_2).$$